

Numerical Solution of a Maximum-Entropy-Based 14-Moment Closure for Multi-Dimensional Flows

Boone R. Tensuda^{1*}, James G. McDonald², & Clinton P. T. Groth¹

¹University of Toronto Institute for Aerospace Studies
4925 Dufferin Street, Toronto, Ontario, Canada, M3H 5T6

²Department of Mechanical Engineering, University of Ottawa
161 Louis Pasteur, Ottawa, Ontario, Canada, K1N 6N5

Abstract: The predictive capabilities of a new, 14-moment, maximum-entropy-based, interpolative closure are explored for multi-dimensional non-equilibrium flows with heat transfer. Unlike the maximum-entropy closure on which it is based, the interpolative closure provides closed-form expressions for the closing fluxes. While still presenting singular solutions in regions of realizable moment space, the interpolative closure proves to have a large region of hyperbolicity while remaining tractable. Furthermore, its singular nature is deemed advantageous for practical simulations. A finite-volume procedure is proposed and described for the numerical solution of the 14-moment closure on two-dimensional computational domains, followed by a presentation and discussion of the results of a numerical dispersion analysis. The first multi-dimensional applications of the closure are then examined for several canonical flow problems in order to provide an assessment of the capabilities of this novel closure for a range of non-equilibrium flows.

Keywords: Non-equilibrium gas dynamics, Transition-regime gas dynamics, Hyperbolic moment closures, Kinetic theory.

1 Introduction & Motivation

The prediction of transition-regime non-equilibrium flows has proven to be a challenging branch of study in computational fluid dynamics (CFD). Transition-regime flows are encountered in a variety of engineering scenarios including: upper atmosphere flight or orbital reentry [1], flows in micro-electromechanical systems (MEMS) [2, 3], chemical vapor deposition in semi-conductor manufacturing, and the study of internal shock structure [4, 5]. These high-Knudsen-number flows cannot be modelled using typical continuum approaches, such as the Euler and Navier-Stokes equations. Traditional methods for modelling non-equilibrium flows, such as direct simulation Monte Carlo (DSMC) methods [6] and techniques involving direct discretization of the Boltzmann equation [7], are limited by their high computational cost, especially when applied in the transition regime. The DSMC technique models a large number of representative particles, and therefore will suffer from slow convergence when many particles are needed. The downfall of solving the discretized Boltzmann equation is its high dimensionality, which leads to high computational cost; especially for physically realistic three-dimensional cases.

The method of moment closures offers an alternative technique for accurately treating transition-regime flows with the potential of greater robustness and a significantly reduced computational cost. The moment closure method considers an assumed form of the particle distribution function to avoid modelling individual particles. It yields an approximation to the Boltzmann equation, which consists of a finite set of partial differential equations (PDEs). These equations are of lower dimensionality compared to the Boltzmann equation, and thus computational cost is reduced. Furthermore, the purely hyperbolic and first-order quasilinear nature of some moment closures also presents several numerical advantages which extend into both the transition and continuum regimes [8]. These hyperbolic systems

*Corresponding author's email: boone.tensuda@mail.utoronto.ca .

are less sensitive to grid irregularities, making them well suited to adaptive mesh refinement (AMR) and complex geometries. They also only require evaluating first derivatives, which means that an extra order of spatial accuracy, relative to a mixed hyperbolic-parabolic type system, can be gained using the same stencil.

A hierarchy of moment closures having a number of desirable properties has been proposed by Levermore based on the maximization of thermodynamic entropy [9, 10]. Unfortunately, complications encountered when considering higher-order moments, such as heat transfer, have severely limited the use of these maximum-entropy closures for general non-equilibrium flows. Recently, new, interpolative-type, maximum-entropy-based, 5-moment (one-dimensional gas) and 14-moment (three-dimensional gas) closures, initially investigated by McDonald and Groth [11], and expanded upon by McDonald and Torrilhon [12], have been proposed that successfully navigate the aforementioned issues. This study will present the results of a further investigation of these new closure techniques via a mathematical dispersion analysis of the governing moment transport equations. The applicability of the 14-moment closure to multidimensional flows will also be examined by solving several two-dimensional canonical flow problems; this study represents the first application of the closure to multi-dimensional flows.

This paper will begin with a summary of relevant gas kinetic theory and the moment closure technique with attention to the maximum-entropy closure hierarchy (Section 2.1). The 14-moment, maximum-entropy-based, interpolative-type closure is presented in Section 3. The finite-volume procedure utilized to solve the 14-moment closure on two-dimensional computational domains is discussed in Section 4.1, and the associated boundary condition technique is presented in Section 4.2. The description and results of a dispersion analysis of the 14-moment system are discussed in Section 5.1, and multi-dimensional cases of Couette flow, conduction between heated flat plates, and subsonic flow past a circular cylinder are presented in Sections 5.2, 5.3, and 5.4, respectively. Finally, conclusions are made based on the results of the dispersion analysis and multi-dimensional flow problems and future work is discussed in Section 6.

2 Background

2.1 Gas Kinetic Theory and Moment Closures

The following section presents the relevant background theory on gas kinetics and moment closures for monatomic gases. When discussing non-equilibrium gases it is convenient to make use of a non-dimensional parameter known as the Knudsen number, Kn . The Knudsen number is defined as the ratio between the mean free path of particles, Λ , and a characteristic length scale, L : $\text{Kn} = \Lambda/L$. Its value is inversely proportional to the frequency of collisions in the gas, and therefore also represents the gases distance from equilibrium. Gases with small Knudsen numbers experience many collisions, and thus will be near equilibrium, this is the so-called continuum regime. Conversely, gases with large Knudsen numbers will have a negligible number of collisions; this is known as the free-molecular regime. The transition regime lies between these two regimes, and presents the largest challenges in modelling. It is in this regime that moment closures show the most promise. Although definitions of the flow regimes vary, typically the continuum regime exists for $\text{Kn} < 0.1$, the transition regime for $0.1 < \text{Kn} < 100$, and the free-molecular regime for $\text{Kn} > 100$.

The method of moment closures relies on the field of gas kinetic theory, which was pioneered by Maxwell and Boltzmann [13, 14]. This theory is built on the concept of a phase-space distribution function, $\mathcal{F}(x_i, v_i, t)$, which represents the probability of finding a single particle with a velocity, v_i , at a position, x_i , at time, t . The most well known of such phase-space distribution functions is the Maxwell-Boltzmann distribution, $\mathcal{M}(v_i)$, which describes the phase-space distribution of a monatomic gas in local thermodynamic equilibrium. All other possible phase-space distributions will tend to evolve toward the Maxwellian over time. This evolution is fully described by the Boltzmann equation [14, 15]

$$\frac{\partial \mathcal{F}}{\partial t} + v_i \frac{\partial \mathcal{F}}{\partial x_i} = \frac{\delta \mathcal{F}}{\delta t}, \quad (1)$$

where $\mathcal{F}(x_i, v_i, t)$ has been written as \mathcal{F} for brevity and it has been assumed that there are no external acceleration fields.

The term $\delta \mathcal{F}/\delta t$ in Equation (1) is known as the collision term, and represents the change of the distribution function as a result of interparticle collisions. It is often formally expressed using the Boltzmann collision integral, which assumes molecular chaos, exclusively binary collisions, and a spherical symmetric force between particles which obeys classical mechanics [15, 16, 17]. However, even with such

assumptions the Boltzmann collision integral is still very complicated and expensive to evaluate. For this reason the simple Bhatnagar–Gross–Krook (BGK) approximation has been used in this study [18]. Using the BGK approximation the collision term becomes

$$\frac{\delta\mathcal{F}}{\delta t} \approx -\frac{\mathcal{F} - \mathcal{M}}{\tau}, \quad (2)$$

where τ is a characteristic relaxation time scale. Although a very simple representation, the BGK approximation maintains the correct collisional invariants at equilibrium ($\mathcal{F} = \mathcal{M}$), and is in agreement with Boltzmann’s H-theorem, meaning the distribution evolves towards the equilibrium Maxwellian. The characteristic relaxation time is approximated as, $\tau = \mu/p$, where μ is the dynamic viscosity of the gas, and p is the hydrostatic pressure. The fact that the BGK collision term uses only a single relaxation time implies that the Prandtl number of the gas considered, Pr , is always unity.

Macroscopic properties of a gas can be found by taking velocity moments of the phase-space distribution function [19]

$$M(x_i, t) = \iiint_{-\infty}^{\infty} mW(v_i)\mathcal{F} \, dv_i = \langle mW(v_i)\mathcal{F} \rangle, \quad (3)$$

where $M(x_i, t)$ is the value of the considered macroscopic property, m is the mass of a gas particle, and $W(v_i)$ is the corresponding velocity weight. The macroscopic moments which will be referred to in this paper are:

$$\begin{aligned} \rho &= \langle m\mathcal{F} \rangle, & \rho u_i &= \langle mv_i\mathcal{F} \rangle, \\ P_{ij} &= \langle mc_i c_j \mathcal{F} \rangle, & Q_{ijk} &= \langle mc_i c_j c_k \mathcal{F} \rangle, \\ R_{ijkl} &= \langle mc_i c_j c_k c_l \mathcal{F} \rangle, & S_{ijklm} &= \langle mc_i c_j c_k c_l c_m \mathcal{F} \rangle, \end{aligned} \quad (4)$$

where ρ is the mass density, u_i is the bulk velocity, $c_i = v_i - u_i$ is the random velocity, P_{ij} is the anisotropic pressure tensor, Q_{ijk} is the generalized heat-flux tensor, and R_{ijkl} and S_{ijklm} represent fourth- and fifth-order moments, respectively. Other convenient macroscopic properties can be related to contractions of these moments,

$$\begin{aligned} p &= \frac{1}{3} \langle mc_i c_i \mathcal{F} \rangle, \\ q_i &= \frac{1}{2} \langle mc_i c_j c_j \mathcal{F} \rangle, \\ r &= \frac{1}{15} \langle mc_i c_i c_j c_j \mathcal{F} \rangle, \end{aligned} \quad (5)$$

where p is the hydrostatic pressure, q_i is the heat-flux vector, and r , the fully contracted fourth-moment, is related to the ‘kurtosis’ of the distribution function.

The transport equations for macroscopic properties are found by taking the appropriate moments of the Boltzmann equation. In general, a set of N transport equations can be found by defining a vector of N velocity weights, $\mathbf{W}(v_i) = [W_0(v_i), W_1(v_i), W_2(v_i), \dots, W_N(v_i)]^T$. The resulting transport equations, known as Maxwell’s equations of change, are

$$\frac{\partial}{\partial t} \langle m\mathbf{W}\mathcal{F} \rangle + \frac{\partial}{\partial x_i} \langle v_i m\mathbf{W}\mathcal{F} \rangle = \langle m\mathbf{W} \frac{\delta\mathcal{F}}{\delta t} \rangle. \quad (6)$$

The first term $\partial\langle m\mathbf{W}\mathcal{F} \rangle/\partial t$ is the rate of change of the solution vector, the second term $\partial\langle v_i m\mathbf{W}\mathcal{F} \rangle/\partial x_i$ is the divergence of the flux of the solution vector, the so-called flux dyad, and the final term $\langle m\mathbf{W}\delta\mathcal{F}/\delta t \rangle$ is the source of the considered macroscopic property resulting from interparticle collisions. It should be noted that the flux dyad always contains moments of one higher order than the solution vector, and thus the equation system is not closed. This implies that in order to solve the Boltzmann equation for an arbitrary phase-space distribution an infinite number of moments must be taken. This is not feasible and approximate methods, which yield a finite set of transport equations, must be used. This technique of approximating the Boltzmann equation using a finite set of transport equations is known as a moment closure.

In order to close the system of moment equations, the unknown closing flux(es) must be related to known moments. Typically this is done by assuming a form for the phase-space distribution which is a function of only known moments. This technique was pioneered by Grad [20], who suggested a distribution of the following form

$$\mathcal{F} = \mathcal{M}[1 + \mathcal{P}^{(N)}(c_i)], \quad (7)$$

where $1 + \mathcal{P}^{(N)}(c_i)$ is a Hermite expansion function about the equilibrium Maxwellian with respect to the random particle velocity [21]. This closure has been applied with success when considering near equilibrium distributions. However, it is possible for the assumed distribution function to become negative, which is nonphysical. Also, as the assumed distribution strays further from equilibrium, there is a loss of hyperbolicity of the resulting moment equations, and a closure breakdown [8]. The Chapman-Enskog closure is an alternative technique which assumes that the distribution is in the form of a small perturbation about the equilibrium Maxwellian distribution [22, 23]. Depending on the order of the perturbation this technique can be used to form the Euler, Navier-Stokes, Burnett, and Super-Burnett equation systems. Since these closures are based on only small perturbations from the Maxwellian, they break down for moderate and large departures from equilibrium.

2.2 Maximum-Entropy Closures

The closures discussed thus far have all arrived at an assumed distribution function through an expansion about the equilibrium distribution. Recently an alternative moment closure technique, known as the maximum-entropy closure, has been proposed [9, 10]. This closure technique assumes a phase-space distribution function which maximizes thermodynamic entropy, and is therefore the most likely distribution, while remaining consistent with a given set of moments. The resulting distribution is,

$$\mathcal{F} = e^{\alpha^T \mathbf{W}}, \quad (8)$$

where α is a set of coefficients that ensure agreement with the moment constraints. The values of the coefficients can be obtained by solving the constrained entropy-maximization problem [9],

$$\frac{\partial}{\partial \alpha} [\langle e^{\alpha^T \mathbf{W}^{(N)}} \rangle - \alpha^T \mathbf{M}^{(N)}] = 0, \quad (9)$$

where \mathbf{M} is a vector of the macroscopic moments considered. This is a numerically expensive problem that must be solved at each flux evaluation.

When solving the maximum-entropy problem, it must be ensured that the phase-space distribution function remains realizable. To ensure moment realizability the given set of moments should, as a minimum, correspond to a set that could arise from a bounded and strictly positive distribution. Physical realizability can be maintained by ensuring that the matrix $\mathbf{Y} = \langle m \mathbf{\Omega} \mathbf{\Omega}^T \mathcal{F} \rangle$ is positive definite [8, 24, 25]. The velocity weighting $\mathbf{\Omega}$ in \mathbf{Y} is chosen such that all considered moments are contained in \mathbf{Y} , and is not necessarily equivalent to \mathbf{W} . Closures of this type offer the advantage of being hyperbolic whenever the maximum-entropy problem can be solved. Since they are not based on an expansion about the Maxwellian they can potentially be applied to gases far from equilibrium.

The two lowest-order members of the maximum-entropy hierarchy are the Maxwellian and Gaussian closures. The Maxwellian closure generates the familiar Euler equation system which is not applicable in non-equilibrium regimes. The Gaussian equation system extends from the Maxwellian by including a non-zero deviatoric stress term, thus viscous effects in non-equilibrium are accounted for [26]. Numerical solutions to the Gaussian closure using Godunov-type finite-volume methods have been studied by Brown *et al.* [27] and McDonald and Groth [8, 28], and generate reliable results in both the continuum and transition regimes when heat transfer is not important. Heat transfer has been introduced in the Gaussian closure using a Chapman-Enskog like expansion by McDonald and Groth [29], however this regularization technique results in the addition of elliptic terms to the moment equations. In order to add heat transfer while maintaining hyperbolicity, super-quadratic velocity weightings must be used in the maximum-entropy distribution's velocity weighting vector, \mathbf{W} .

Unfortunately, issues with the maximum-entropy closure arise when higher-order, super-quadratic, velocity terms, which describe heat transfer, are added. Firstly, the maximum-entropy problem ceases to have a closed-form analytic solution and relatively expensive iterative approaches would be required to relate macroscopic moments and closure coefficients. Furthermore and more limiting, regions in physically realizable moment space develop within which the maximum-entropy problem cannot be solved as the approximate distribution does not remain bounded [30]. This unrealizable subspace will be referred to as the Junk subspace. These complications have limited the use of the maximum-entropy closure technique for general non-equilibrium flows. However, a new interpolative-type closure [12, 24], has shown success in navigating these issues and is the primary focus of the present study.

3 The 14-Moment Interpolative Closure

As mentioned above, recently an interpolative-type closure based on the maximum-entropy hierarchy has been proposed [12, 24]. The velocity weighting vector used for this closure is $\mathbf{W} = [1, v_i, v_i v_j, v_i \mathbf{v}^2, \mathbf{v}^4]$, where $\mathbf{v} = v_i v_i$. For a monatomic gas, this leads to a set of 14-moment equations, which include a non-zero heat-flux vector, in the form

$$\frac{\partial \mathbf{U}}{\partial t} + \frac{\partial \mathbf{F}_k}{\partial x_k} = \mathbf{S}, \quad (10)$$

where \mathbf{U} is the vector of conserved variables, \mathbf{F}_k is the flux dyad, and \mathbf{S} is the source vector resulting from interparticle collisions modelled using the BGK operator. For a three-dimensional gas, these vectors are

$$\mathbf{U} = \begin{pmatrix} \rho \\ \rho u_i \\ \rho u_i u_j + P_{ij} \\ \rho u_i u_j u_j + u_i P_{jj} + 2u_j P_{ij} + Q_{ijj} \\ \rho u_i u_i u_j u_j + 2u_i u_i P_{jj} + 4u_i u_j P_{ij} + 4u_i Q_{ijj} + R_{iijj} \end{pmatrix}, \quad (11)$$

$$\mathbf{F}_k = \begin{pmatrix} \rho u_k \\ \rho u_i u_k + P_{ik} \\ \rho u_i u_j u_k + u_i P_{jk} + u_j P_{ik} + u_k P_{ij} + Q_{ijk} \\ \rho u_i u_k u_j u_j + u_i u_k P_{jj} + 2u_i u_j P_{jk} + 2u_j u_k P_{ij} + u_j u_j P_{ik} + u_i Q_{kjj} + u_k Q_{ijj} + 2u_j Q_{ijk} + R_{ikjj} \\ \rho u_k u_i u_i u_j u_j + 2u_k u_i u_i P_{jj} + 4u_i u_i u_j P_{jk} + 4u_i u_j u_k P_{ij} + 2u_i u_i Q_{kjj} + 4u_i u_k Q_{ijj} + 4u_i u_j Q_{ijk} \\ + 4u_i R_{ikjj} + u_k R_{iijj} + S_{kiiij} \end{pmatrix}, \quad (12)$$

$$\mathbf{S} = \begin{pmatrix} 0 \\ 0 \\ \frac{\delta_{ij} P_{kk} - 3P_{ij}}{3\tau} \\ \frac{2u_i (\delta_{ij} P_{kk} - 3P_{ij}) - 6u_i P_{jk} - 3Q_{ijj}}{3\tau} \\ \frac{1}{3\tau} \left(-3R_{iijj} + \frac{5P_{ii} P_{jj}}{\rho} - 12u_i Q_{ijj} + 4u_i u_j (\delta_{ij} P_{kk} - 3P_{ij}) \right) \end{pmatrix}. \quad (13)$$

It should be noted that the 14-moment system as presented above is not closed; to close the system the moments Q_{ijk} , R_{ijkk} , and S_{ijjkk} in the flux vector must be approximated. In order to navigate the issues associated with higher-order maximum-entropy closures, the interpolative closure of McDonald and Torrillon [12] approximates these closing fluxes using closed-form expressions, as opposed to numerically solving the maximum-entropy problem. These closed-form expressions are found in three steps. Firstly, the region of realizability between the physical realizability boundary and Junk-subspace is determined, and a suitable remapping of moments is employed. Information about the behaviour of the closing flux is then found at equilibrium and on the realizability boundaries. Finally, a closing flux is postulated which is consistent with the constraints at the boundaries and also transitions between them with values that approximate those found by solving the maximum-entropy problem numerically. The reader should refer to the paper by McDonald and Torrillon [12] for additional information on the derivation of the 14-moment system and the closing fluxes.

It is convenient when forming the closing fluxes to define a parabolic surface mapping using an additional variable, σ , where σ represents paraboloids in realizable moment space, with $\sigma = 1$ corresponding to the physically realizable boundary, and $\sigma = 0$ corresponding to the Junk subspace. In this case, σ is related to the know moments such that the following equality is satisfied,

$$R_{iijj} = \frac{1}{\sigma} Q_{kii} (P^{-1})_{kl} Q_{ljj} + \frac{2(1-\sigma) P_{ji} P_{ij} + P_{ii} P_{jj}}{\rho} \quad \sigma \in [0, 1]. \quad (14)$$

Expressions for the closing fluxes as a function of know moments can then be postulated using the interpolative method summarized above and fully described in [12]. The resulting closing fluxes are

$$Q_{ijk} = \frac{\partial Q_{ijk}}{\partial Q_{mnn}} Q_{mnn}, \quad (15)$$

where

$$\frac{\partial Q_{ijk}}{\partial Q_{mnn}} = \frac{P_{il}(P^2)_{jk} + P_{kl}(P^2)_{ij} + P_{jl}(P^2)_{ik}}{P_{lm}(P^2)_{\alpha\alpha} + 2(P^3)_{lm}}, \quad (16)$$

$$R_{ijkk} = \frac{1}{\sigma} Q_{ijl}(P^{-1})_{lm} Q_{mkk} + \frac{2(1-\sigma)P_{ik}P_{kj} + P_{ij}P_{kk}}{\rho}, \quad (17)$$

$$S_{ijjkk} = \frac{Q_{npp}Q_{mjj}Q_{ikl}}{\sigma^2 P_{kn}P_{lm}} + 2\sigma^{\frac{1}{2}} \frac{P_{jj}Q_{ikk}}{\rho} + (1-\sigma^{\frac{1}{2}})W_{im}Q_{mnn}, \quad (18)$$

and where

$$W_{im} = \frac{1}{\rho P_{lm}(P^2)_{\alpha\alpha} + 2(P^3)_{lm}} \left[P_{il}(P_{\alpha\alpha})^3 + 6P_{il}(P^3)_{\alpha\alpha} + 7(P^2)_{\alpha\alpha}(P^2)_{il} \right. \\ \left. + 10P_{\alpha\alpha}(P^3)_{il} + 10(P^4)_{il} - (P^2)_{\alpha\alpha}P_{\beta\beta}O_{il} - 3(P_{\alpha\alpha})^2(P^2)_{il} \right]. \quad (19)$$

By inspection of Equation (17), it is clear that a singularity in the closing flux continues to be encountered at the Junk subspace (when $\sigma=0$), as was also the case in the original maximum-entropy closures. However, past research has found that this singular nature is advantageous in practical implementation [12]. It produces very large propagation speeds and was found to yield accurate solutions of stationary, one-dimensional, shock structure having smooth transitions, without undesirable sub-shocks, even for high Mach numbers [12]. The effect of the singularity on wave propagation speed is further explored in Section 5.1.

4 Numerical Solution of the 14-Moment Closure

4.1 Upwind Finite-Volume Scheme

The moment transport equation system of the 14-moment closure for two-dimensional planar flows on multi-block quadrilateral meshes is solved using a parallel higher-order Godunov-type finite-volume scheme. As the continuum regime is approached the values of the relaxation time, τ , can become very small, leading to excessive numerical stiffness of the system. This issue is alleviated by utilizing point-implicit time-marching [28]. The resulting fully-discrete solution scheme which is applied to cell (i, j) is

$$\tilde{\mathbf{U}}_{(i,j)}^{n+1} = \mathbf{U}_{(i,j)}^n - \frac{\Delta t}{A_{(i,j)}} \left(\sum_k (\mathbf{F}_k \cdot n_k \Delta l)_{(i,j,k)}^n \right) + \Delta t \tilde{\mathbf{S}}_{(i,j)}^{n+1}, \quad (20)$$

$$\mathbf{U}_{(i,j)}^{n+1} = \mathbf{U}_{(i,j)}^n - \frac{\Delta t}{2A_{(i,j)}} \left(\sum_k (\mathbf{F}_k \cdot n_k \Delta l)_{(i,j,k)}^n + \sum_k (\tilde{\mathbf{F}}_k \cdot n_k \Delta l)_{(i,j,k)}^{n+1} \right) + \Delta t \left(\frac{\mathbf{S}_{(i,j)}^n + \mathbf{S}_{(i,j)}^{n+1}}{2} \right), \quad (21)$$

where $\mathbf{U}_{(i,j)}^n$ and $\mathbf{S}_{(i,j)}^n$ are the solution vector of conserved variables and source vector, respectively, in cell (i, j) at time step n , \mathbf{F}_k is the flux dyad, Δl is the length of the cell face, n_k is the unit vector normal to the cell face, $A_{(i,j)}$ is the area of cell (i, j) , and Δt is the time step.

The term, $(\mathbf{F}_k \cdot n_k \Delta l)_{(i,j,k)}$, is the numerical flux at the cell faces, which is found by solving Riemann problems at the corresponding cell interfaces. The left and right solution states at the cell interfaces required to solve the Riemann problem are found by extrapolating the cell-averaged quantities using a least-squares piece-wise limited linear solution reconstruction technique, with the Venkatakrisnan type limiter [31]. The HLL-type approximate Riemann solver [32] is then used to find a solution to the Riemann problem, and thus a numerical flux. Using the HLL technique the intermediate flux at the cell interface, \mathbf{F}^{HLL} , is found as

$$\mathbf{F}^{\text{HLL}} = \frac{\lambda^+ \mathbf{F}_L - \lambda^- \mathbf{F}_R}{\lambda^+ - \lambda^-} + \frac{\lambda^+ \lambda^-}{\lambda^+ - \lambda^-} (\mathbf{U}_R - \mathbf{U}_L), \quad (22)$$

where \mathbf{F}_R and \mathbf{F}_L are the right and left fluxes, \mathbf{U}_R and \mathbf{U}_L are the right and left solution states, and λ^+ and λ^- are the maximum and minimum solution wave propagation speeds, respectively. Typically, the maximum and minimum wave speeds are found using the eigenvalues of the flux Jacobian. However, due

to the complexity of the 14-moment system, at this stage in development the maximum and minimum wave speeds are approximated based on the acoustic wave speeds in a monatomic gas. The approximate wave speeds at a cell interface with a normal in the x -direction are

$$\lambda^- = \min \left(u_x^{(R)} - \xi \sqrt{\frac{\gamma P_{xx}^{(R)}}{\rho^{(R)}}}, u_x^{(L)} - \xi \sqrt{\frac{\gamma P_{xx}^{(L)}}{\rho^{(L)}}} \right), \quad (23)$$

$$\lambda^+ = \max \left(u_x^{(R)} + \xi \sqrt{\frac{\gamma P_{xx}^{(R)}}{\rho^{(R)}}}, u_x^{(L)} + \xi \sqrt{\frac{\gamma P_{xx}^{(L)}}{\rho^{(L)}}} \right), \quad (24)$$

where the superscripts (R) and (L) denote properties at the right and left states, respectively, γ is the ratio of specific heats and equal to 5/3 for a monatomic gas, and ξ is a tuning coefficient which is set large enough that the scheme is stable, while remaining small enough to ensure there is not excess numerical dissipation or excessively small time steps. Due to the singular nature of the closure flux Jacobians and numerical limitations, the values of σ must be limited, a lower limit of $\tilde{\sigma} = 2.0 \times 10^{-4}$ is found to be sufficient. If σ becomes less than this value, it is then replaced with $\sigma = \tilde{\sigma}$.

4.2 Boundary Conditions

Appropriate solid-wall boundary conditions for moment closure techniques, which produce the correct non-equilibrium phenomena, are not obvious. Determining the boundary conditions at a solid wall is simplified by assuming that a Knudsen layer of infinitesimal thickness forms adjacent to the wall [20]. In this Knudsen layer, the particle distribution function is a combination of the distribution function of particles from the interior flow field and particles reflected from the solid wall. It is also assumed that particle reflection is either specular or diffusive. The probability of a diffusive interaction occurring is defined using an accommodation coefficient, a . When $a = 0$, the interactions will only be specular, and particles will experience an elastic collision with the wall. When $a = 1$, the interactions will be exclusively diffusive, and particles will be fully accommodated by the wall before being reintroduced into the Knudsen layer with a Maxwellian distribution which depends on the wall's temperature and velocity.

Using these assumptions, a distribution function for the particles at the solid-wall boundary can be defined as

$$\mathcal{F}_{\text{Kn}} = \mathcal{F}_+ + \mathcal{F}_-, \quad (25)$$

where \mathcal{F}_{Kn} is the distribution of particles in the Knudsen layer, \mathcal{F}_- is the distribution of the particles entering the Knudsen layer from the interior flow field, and \mathcal{F}_+ is the distribution of the reflected particles. Assuming that the wall lies parallel to the y -axis (see Figure 1), these distribution functions are

$$\mathcal{F}_- = \begin{cases} \mathcal{F}_{\text{int}}(v_x, v_y, v_z) & \text{if } v_x > 0, \\ 0 & \text{if } v_x < 0 \end{cases} \quad (26)$$

$$\mathcal{F}_+ = \begin{cases} a\mathcal{M}_W(v_x, v_y, v_z) + (1-a)\mathcal{F}_{\text{int}}(-v_x, v_y, v_z) & \text{if } v_x < 0, \\ 0 & \text{if } v_x > 0 \end{cases} \quad (27)$$

where \mathcal{F}_{int} is the distribution function of particles in the interior flow, and \mathcal{M}_W is the Maxwellian distribution of the particles accommodated by the wall,

$$\mathcal{M}_W = n_w \left(\frac{m}{2\pi k T_w} \right)^{\frac{3}{2}} e^{-\frac{m}{2k T_w} (v_x^2 + (v_y - u_{wy})^2 + v_z^2)}, \quad (28)$$

where T_w is the temperature of the wall, u_{wy} is the wall velocity, and n_w is the number density of the reflected Maxwellian. These distributions are used in conjunction with known properties at the wall, such as zero normal net flux, to find expressions for the moments in the Knudsen layer, and approximate boundary conditions are formed based on these moments.

Since the 14-moment closure is formulated by postulating relations between the closing fluxes and known moments directly, as opposed to assuming a certain distribution function, it is not obvious what form should be used for the interior flow distribution, \mathcal{F}_{int} . However, since the closure is based on the maximum-entropy closure, it would be expected that the internal distribution would be near to a maximum-entropy distribution. For the purposes of generating some first numerical solutions to the

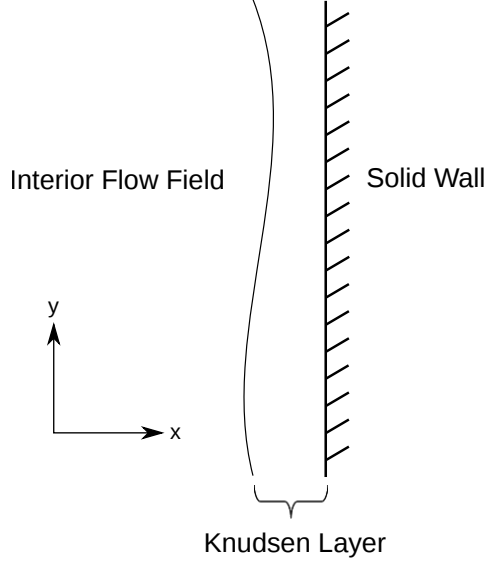


Figure 1: *Representation of the Knudsen layer.*

14-moment closure, a Gaussian distribution, corresponding to a 10-moment maximum-entropy closure, is used in this study as the interior distribution. By defining an anisotropic ‘temperature’ tensor, $\Theta_{ij} = P_{ij}/\rho$, the Gaussian distribution, \mathcal{G} , can be expressed as,

$$\mathcal{G} = \frac{\rho}{m(2\pi)^{3/2}(\det\Theta_{ij})^{1/2}} \exp\left(-\frac{1}{2}\Theta_{ij}^{-1}c_i c_j\right). \quad (29)$$

The resulting moments of the Knudsen layer distribution, \mathcal{F}_{Kn} , which the approximate boundary conditions are based upon, are:

$$u_{x\text{Kn}} = 0, \quad (30)$$

$$u_{y\text{Kn}} = (2-a) \left[\frac{u_y}{2} + \frac{P_{xy}}{\sqrt{2\pi\rho P_{xx}}} \right] + \frac{a}{2} \sqrt{\frac{P_{xx}}{n_w k T_w}} u_{wy}, \quad (31)$$

$$P_{xy\text{Kn}} = a \left[\frac{P_{xy}}{2} + \sqrt{\frac{\rho P_{xx}}{2\pi}} (u_y - u_{y\text{Kn}}) - \sqrt{\frac{\rho_w n_w k T_w}{2\pi}} (u_{wy} - u_{y\text{Kn}}) \right], \quad (32)$$

$$Q_{xii\text{Kn}} = Q_{xxx\text{Kn}} + Q_{xyy\text{Kn}} + Q_{xzz\text{Kn}}, \quad (33)$$

where

$$Q_{xxx\text{Kn}} = -amn_{\text{int}} \sqrt{\frac{2}{\pi} \left(\frac{P_{xx}}{\rho} \right)^3} + amn_w \sqrt{\frac{2}{\pi} \left(\frac{kT_w}{m} \right)^3}, \quad (34)$$

$$\begin{aligned} Q_{xyy\text{Kn}} = & -amn_{\text{int}} \sqrt{\frac{1}{2\pi} \left(\frac{P_{xx}}{\rho} \right)} \left[\frac{P_{xx}P_{yy} + P_{xy}^2}{P_{xx}\rho} - \frac{P_{xy}}{P_{xx}} (u_y - u_{y\text{Kn}}) \sqrt{2\pi \left(\frac{P_{xx}}{\rho} \right)} + (u_y - u_{y\text{Kn}})^2 \right] \\ & + amn_w \sqrt{\frac{kT_w}{2\pi m}} \left(\frac{kT_w}{m} + (u_{wy} - u_{y\text{Kn}})^2 \right), \end{aligned} \quad (35)$$

and

$$Q_{xzz\text{Kn}} = -amn_{\text{int}} \sqrt{\frac{1}{2\pi} \left(\frac{P_{xx}}{\rho} \right)} \left(\frac{P_{zz}}{\rho} \right) + amn_w \sqrt{\frac{2}{\pi} \left(\frac{kT_w}{m} \right)^3}, \quad (36)$$

where n_{int} is the number density of the interior distribution. While not completely consistent with

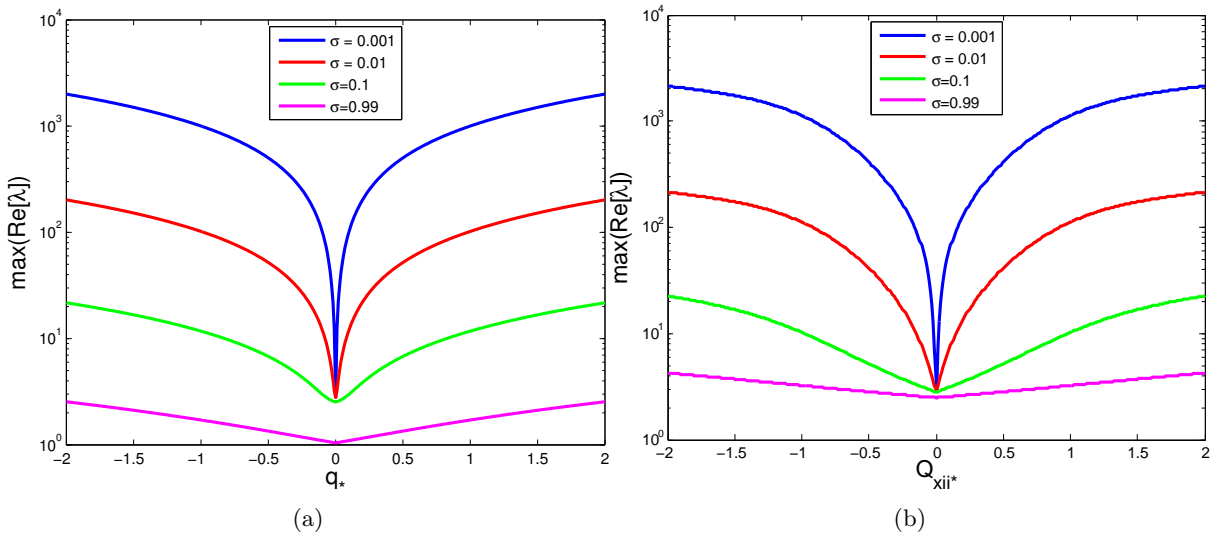


Figure 2: *Maximum wave speed on constant σ contours for a (a) one-dimensional gas and (b) three-dimensional gas with spatial variations in one direction.*

the 14-moment interpolative closure, the present boundary scheme has allowed the exploration of multi-dimensional solutions to the closure.

5 Numerical Results

5.1 Dispersion Analysis and Maximum Wavespeeds

Recall that the solutions of hyperbolic relaxation systems of PDEs are in the form of waves. Therefore, when studying systems of such equations understanding the properties of these waves is of great importance. Two such properties are the wave speed and damping rate. The PDE systems considered in moment closures exhibit dispersive wave behaviours, meaning that their wave speeds and damping are a function of the wavenumber of the propagating solution wave. In order to gain insight into what these wave speeds and damping rates are, and how they vary with wavenumber, a dispersion analysis is performed. In general, a dispersion analysis describes how a certain linear operator acts on Fourier modes of perturbations with different wave numbers [33]. In the case of a system of PDEs in weakly conservative form this linear operator is $\partial/\partial t + \mathbf{A}\partial/\partial x - \mathbf{Q}$, where \mathbf{A} is the flux Jacobian, and \mathbf{Q} is the source term Jacobian. The perturbative solutions are assumed to be of the form

$$\mathbf{u}(x, t) = \text{Re} \left[\mathbf{v}(t)e^{(-ikx)} \right], \quad (37)$$

where, $\mathbf{v}(t)$ is the amplitude of the solution wave, k is the wavenumber, and i is $\sqrt{-1}$. The linearized differential operator applied to Equation (37) yields a set of ordinary differential equations (ODEs) given by

$$\frac{d\mathbf{v}}{dt} = (ik\mathbf{A} + \mathbf{Q})\mathbf{v}, \quad (38)$$

which has the non-trivial solution

$$\mathbf{v}(t) = e^{it(k\mathbf{A} + \mathbf{Q})} \mathbf{u}_0, \quad (39)$$

where \mathbf{u}_0 is the initial amplitude of the solution. The wave speed and decay constants of this solution are proportional to the real and imaginary components of the eigenvalues of $(k\mathbf{A} - i\mathbf{Q})$, respectively. The wavenumber k can be related to the Knudsen number by $\text{Kn} = 2\pi k$ [27], and therefore the properties of the solution waves can be determined for the entire range of Knudsen numbers.

Dispersion analyses, which are outlined above, were applied to the interpolative closure for a monatomic one-dimensional gas, meaning gas particle velocity is confined to a single direction, as well as a monatomic three-dimensional gas with only variations in the x -direction and an axi-symmetric distribution func-

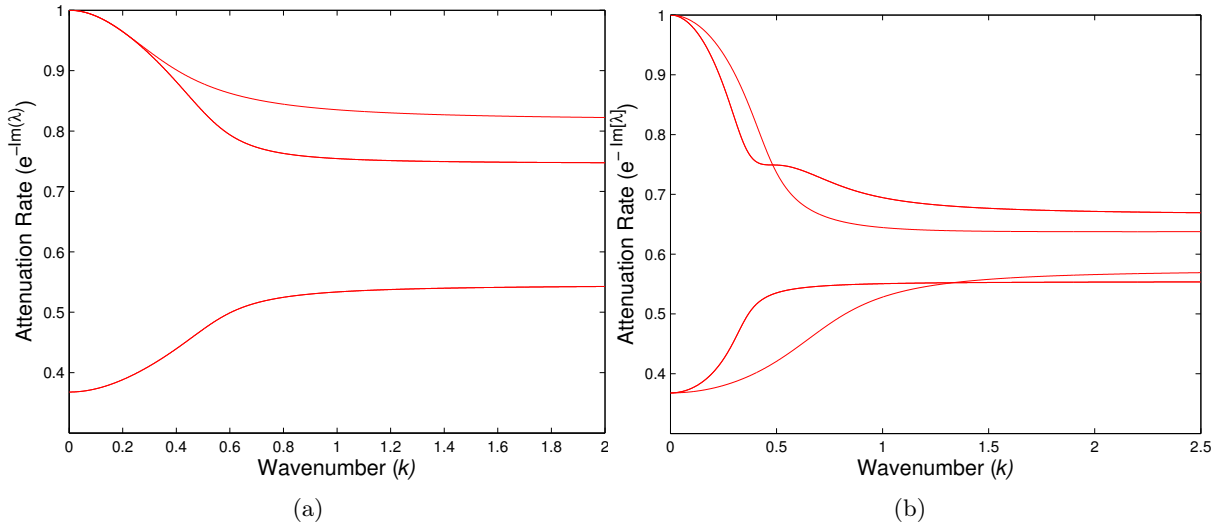


Figure 3: Attenuation rate diagrams for a (a) one-dimensional and (b) three-dimensional gas near equilibrium.

tion about the v_x axis, leading to moment relations: $u_x = u_y = 0$, $P_{xy} = P_{xz} = P_{yz} = 0$, and $Q_{yji} = Q_{zji} = 0$. The particle distribution function is transformed such that $u_x = 0$, and the moments are non-dimensionalized such that $\rho = p = 1$ in the one-dimensional gas, and $\rho = P_{xx} = P_{yy} = P_{zz} = 1$ in the three-dimensional gas, these non-dimensionalized moments are denoted with a ‘ \star ’ subscript.

Of particular interest are the maximum frozen wave speeds, since these values will limit the Mach numbers for which internal shock structures can be resolved without generating unphysical sub-shocks. For the Grad-13 and Gaussian closure the maximum frozen wave speeds at equilibrium have been found to be Mach 1.65 [10] and Mach $3/\sqrt{5}$ [27], respectively. The 14-moment closure however has been found to provide smooth shock structure even up to Mach numbers of 8 [12]. It is expected that the singularity in the closing flux encountered at the Junk subspace results in arbitrarily large frozen wave speeds as the subspace is approached, leading to smooth shock structures. This is confirmed by the dispersion analysis of the 14-moment system as shown in Figure 2, which display the maximum frozen wave speeds on constant σ contours. Recall that σ is equal to zero at the Junk subspace, therefore the maximum wave speed is expected to increase as σ approaches zero, as is seen in Figure 2, although it is observed that the wave speeds reduce rapidly at points below equilibrium. The dispersion analysis is also performed at a single point very close to equilibrium, since the presence of the Junk subspace prevents analysis exactly at equilibrium. The attenuation rate results are shown in Figure 3. It is clear that these attenuation values remain between zero and one for all wavenumbers and thus the system is stable for both one- and three-dimensional gases, and all flow regimes in terms of the Knudsen number.

5.2 Couette Flow

A good first test case for non-equilibrium models is that of planar subsonic Couette flow between two oppositely moving plates as studied previously by McDonald and Groth [28, 8] and McDonald *et al.* [11]. The Knudsen number for this case is found as $\text{Kn} = \Lambda/d$ where d is the distance between the plates, and the mean free path is given by

$$\Lambda = \frac{16\mu}{5\sqrt{2\pi\rho p}}. \quad (40)$$

This model of the mean free path assumes that the gas molecules interact as hard spheres [6]. For this case, the Knudsen number can be adjusted by simply changing the distance between the plates. It is expected that as the Knudsen number is raised, and the free-molecular regime is approached, the appearance of slip flow at the plates will become more pronounced, since fewer interactions between the gas and plate particles are occurring. The ability to recreate this slip flow accurately is a good benchmark for both the moment closure method and the boundary conditions considered.

The Couette flow case which has been considered consists of two parallel plates moving in opposite directions at a velocity, U , of 30 m/s in the x -direction. The gas between the plates is argon with

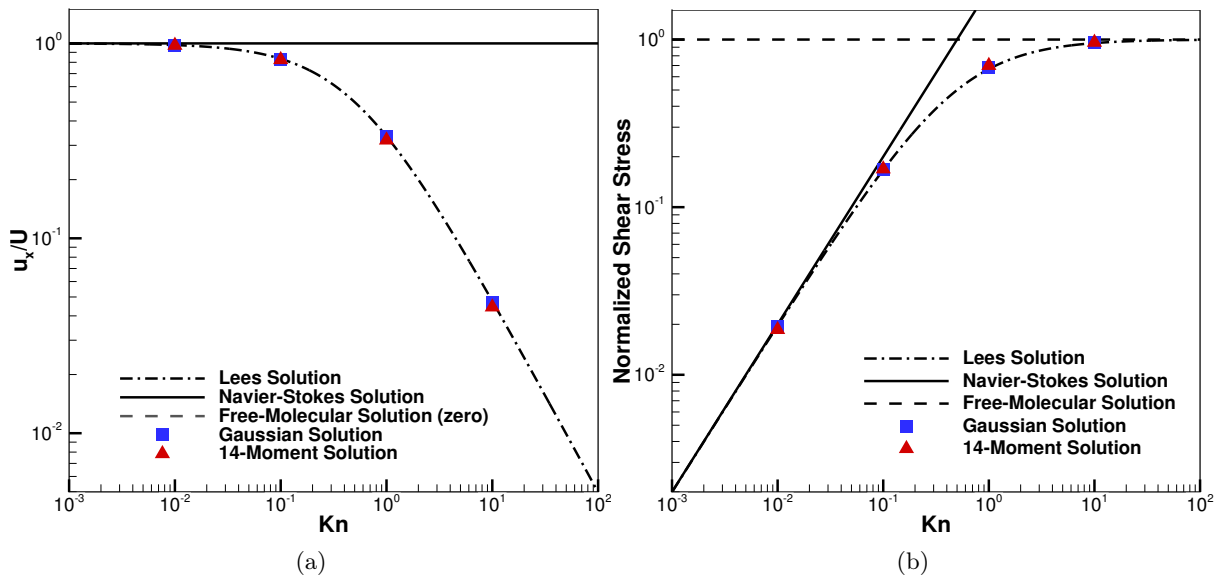


Figure 4: (a) Normalized flow velocity at the plate as a function of Knudsen number. (b) Normalized shear stress between the plates as a function of Knudsen number.

standard atmospheric free stream density of 1.225 kg/m^3 and pressure of 101.325 kPa , and therefore a temperature of 397.37 K . The transport equations of the 14-moment closure, summarized in Section 3, were solved using the numeric algorithm described in Section 4.1, on a mesh containing 20 cells in the x -direction, and 200 cells in the y -direction, for a total of 4000 computational cells. Periodic boundaries were specified in the x -direction and the solid-wall boundary conditions, Equations (30)-(32), were specified at the plate surfaces. Since heat transfer was not expected to be significant for this case, a simple reflection boundary condition was specified for the heat flux. A CFL number of 0.5 and an accommodation coefficient of $a = 1$ were used for both the Couette flow and conduction between heated plates simulations. The results for the normalized flow velocity u_x/U , and normalized shear stress

$$P_{xy}^* = \frac{-P_{xy}}{\rho U \sqrt{\frac{2kT}{\pi m}}}, \quad (41)$$

for a wide range of Knudsen numbers are shown in Figure 4. These computed values are compared in the figure with results found using the Gaussian closure [8], and the analytical solution developed by Lees [34]. It is evident that the predicted values of the 14-moment closure are in very good agreement with those of the Gaussian and Lees' solution throughout the continuum, transition, and free-molecular regimes. The figures also illustrate the failure of both the Navier-Stokes equations and free-molecular solution in the transition regime, emphasizing the importance of moment closures and their ability to model gases throughout this regime.

5.3 Conduction Between Heated Plates

The case of heat conduction between two infinite flat plates oriented parallel to the x -axis has also been considered. Since the effects of heat transfer are now expected to be significant, the use of a simple reflection boundary condition, such as that used for the planar Couette flow case considered in Section 5.2, is no longer justified. The more appropriate solid-wall half-Maxwellian boundary condition, Equations (33)-(36), is used instead. In this case it is expected that in the continuum regime the temperature of the interior fluid adjacent to the wall will be equivalent to the wall temperature. However, as the Knudsen number is increased a temperature jump between the wall and internal fluid will develop, due to the reduced number of interactions between the gas and plate particles. Accurately predicting this phenomena is a good benchmark for the 14-moment closure and heat-flux boundary conditions.

The gas considered between the heated plates is argon at a temperature of 397.37 K , and standard atmospheric free stream density and pressure. The upper plate temperature, T_U , has been set to 407.37 K , and the lower plate temperature, T_L , has been set to 387.37 K ; resulting in a temperature differential of 20 K between the plates. The computational domain consisted of 10 cells in the x -direction and 100

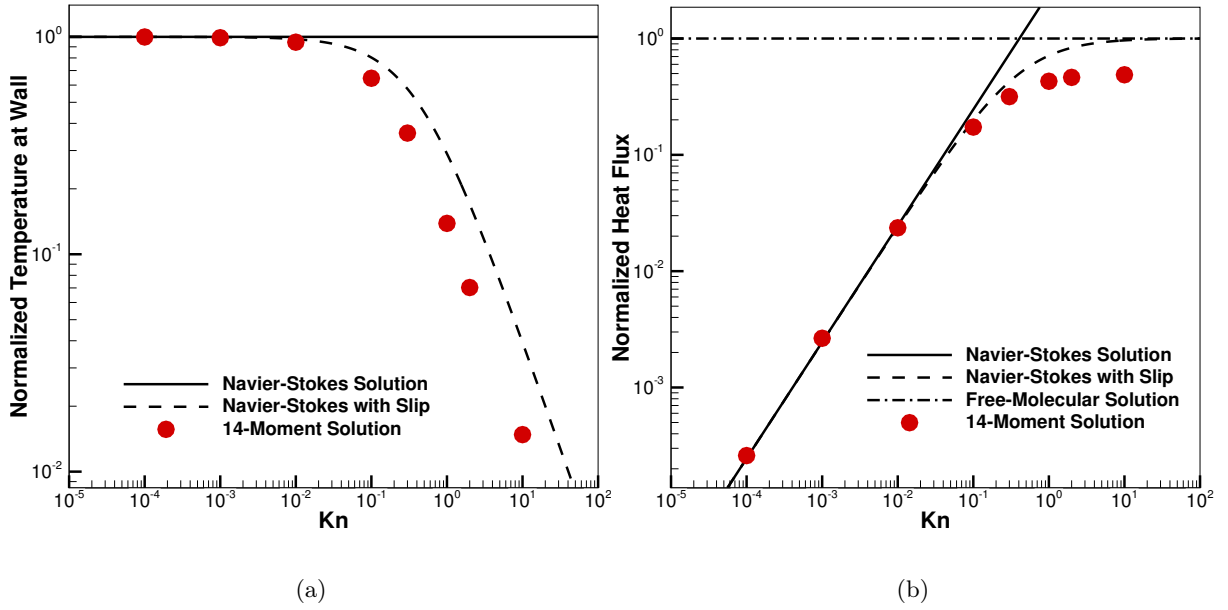


Figure 5: (a) Normalized temperature at the wall with respect to Knudsen number. (b) Heat flux between the plates, normalized with respect to the free-molecular value, with respect to Knudsen number.

cells in the y -direction, for a total of 1000 computational cells. The solid-wall half-Maxwellian boundary condition were specified at the plate surfaces, and periodic boundaries were used in the x -direction. The values of normalized wall temperature, T^* , and normalized heat flux between the plates were found for a large range of Knudsen numbers.

The numerical results for heat transfer between the two plates are presented in Figure 5. In the figure, the wall temperature has been normalized as

$$T^* = \frac{T - T_m}{T_w - T_m}, \quad (42)$$

where T is the temperature of the gas at the wall, T_m is the gas temperature midway between the plates, and T_w is the temperature of the plate. The heat flux between the plates has been normalized with respect to the free-molecular heat flux [35, 36]

$$q_x = \rho_m \sqrt{\frac{RT_m}{2\pi}} \left(c_v + \frac{1}{2}R \right) (T_U - T_L), \quad (43)$$

where ρ_m is the density of the gas midway between the plates, R is the specific gas constant, and c_v is the heat capacity at constant volume. The results are compared to the free-molecular solution, the continuum Navier-Stokes solution, and the Navier-Stokes solution with temperature jump boundary conditions. The temperature jump distance, g , is found as

$$g = \frac{2 - a}{a} (2\pi RT)^{\frac{1}{2}} \frac{K}{(\gamma + 1) c_p}, \quad (44)$$

where K is the thermal conductivity. In order to stay consistent with the BGK approximation the thermal conductivity is taken to be $K = c_p \mu$, where c_p is the heat capacity at constant pressure, thus ensuring a Prandtl number of unity.

The results of Figure 5 show some of the expected characteristics for this case. The normalized temperature results, Figure 5 (a), display the expected temperature jump beginning in the transition region, however it is clear that the 14-moment solution somewhat over predicts the temperature jump, relative to the Navier-Stokes solution with temperature jump boundary conditions, at $\text{Kn} > 0.01$. The results for normalized heat flux, Figure 5 (b), show the correct prediction in the continuum regime, however plateau to a value less than the expected free-molecular heat flux. It is expected that these results would be significantly improved by determining the heat-flux boundary conditions based on an interior distribution which is more consistent with the 14-moment closure. For instance a Grad-like perturbation of the Gaussian distribution could be considered [37, 38].

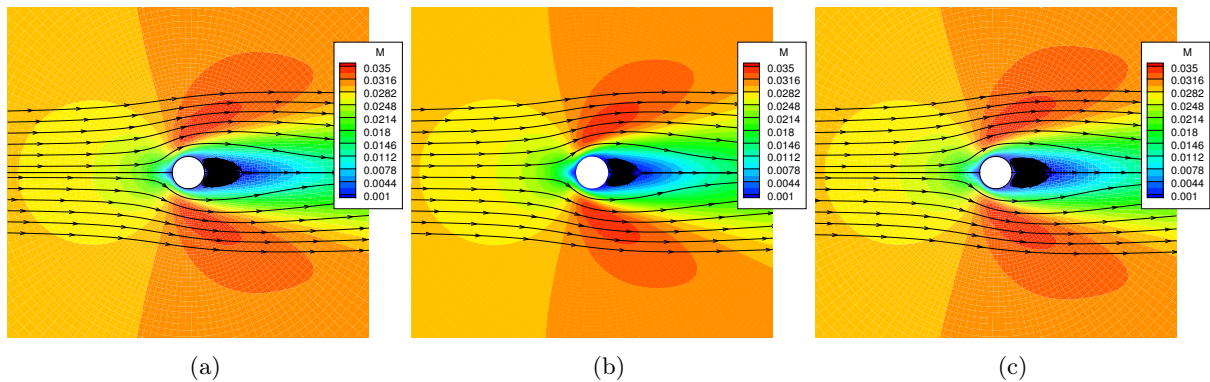


Figure 6: Mach contours and velocity streamlines for subsonic flow past a circular cylinder at $Kn=0.002$ found by solving the (a) Gaussian, (b) regularized Gaussian, and (c) 14-moment closures.

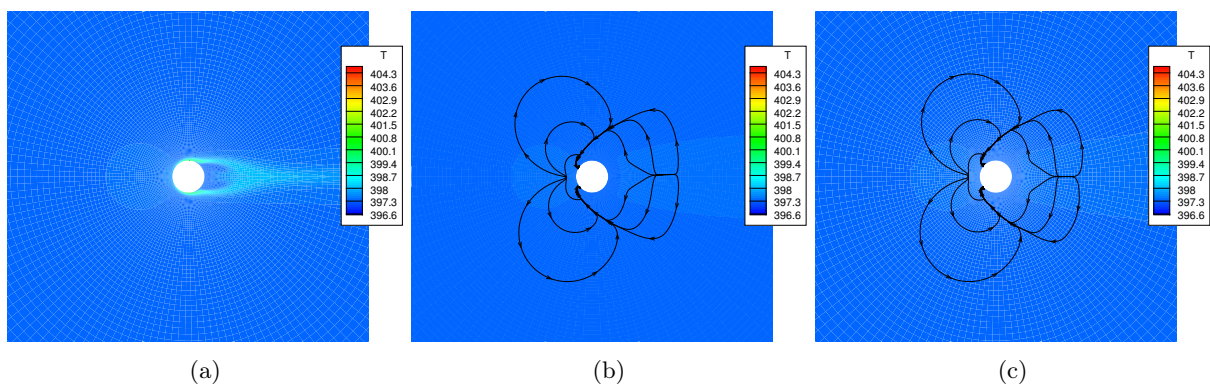


Figure 7: Temperature contours and heat-flux streamlines for subsonic flow past a circular cylinder at $Kn=0.002$ found by solving the (a) Gaussian, (b) regularized Gaussian, and (c) 14-moment closures.

5.4 Subsonic Flow Past a Circular Cylinder

Subsonic flow past a circular cylinder has been considered for both a continuum, $Kn=0.002$, and transition, $Kn=0.1$, regime flow. For comparison, the problems were also solved using the Gaussian [8, 28] and regularized Gaussian [8, 29] closures. The regularized Gaussian closure incorporates anisotropic thermal-diffusion effects using added elliptic terms. For all cases the gas considered was argon at standard atmospheric density and pressure, and a temperature of 397.37 K. Solutions were found using each closure technique on a quadrilateral, body fitted, computational mesh of 125 cells in the radial direction, and 150 cells in the azimuthal direction, for a total of 18 750 computational cells. The mesh was stretched resulting in a much greater concentration of cells near the cylinder surface. Similar mesh sizes have been used in previous studies of moment closure solutions for subsonic flow past a circular cylinder by McDonald [39], and found to be sufficient. The speed ratio, S , defined as the ratio between the free stream gas speed and the most probable particle speed, was 0.027. Once again an accommodation coefficient of $a = 1$ was used. The temperature of the cylinder was set equivalent to the free-stream gas temperature of 397.37 K.

5.4.1 Results for $Kn=0.002$

Solutions found for the continuum case, $Kn=0.002$, are presented in Figures 6 and 7. For this case the Reynolds number is 24.3728. It can be seen that the Mach number contours are very similar for each of the solution methods, as is expected. Since this case is in the continuum regime, negligible velocity slip is observed at the surface of the cylinder. The velocity streamlines show the formation of a recirculation region downstream of the cylinder. This is a well established phenomena at the Reynolds number considered. Since the gas is close to local thermodynamic equilibrium for this low Knudsen number case the variations in temperature are small, however the Gaussian solution shows slightly higher temperatures near the cylinder, signifying that even for this continuum regime case heat transfer is starting to have an effect. The regularized Gaussian and 14-moment closure solutions are in good

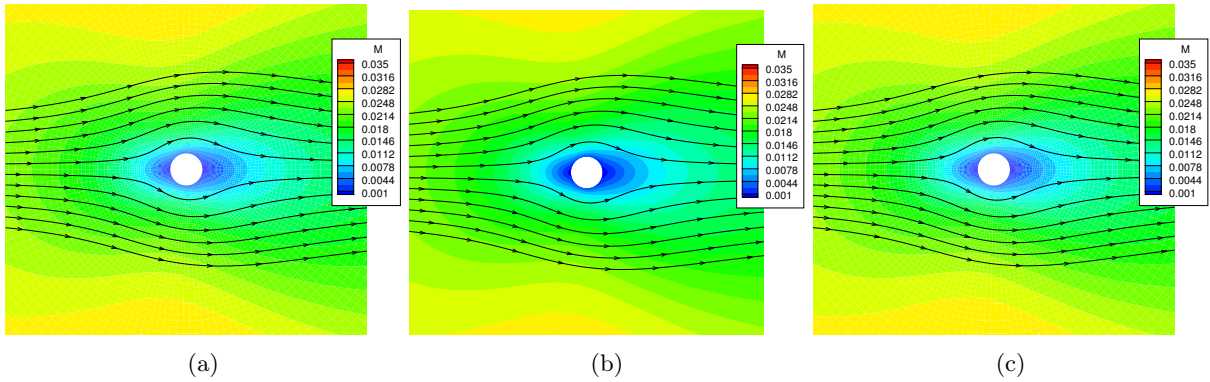


Figure 8: Mach contours and velocity streamlines for subsonic flow past a circular cylinder at $Kn=0.1$ found by solving the (a) Gaussian, (b) regularized Gaussian, and (c) 14-moment closures.

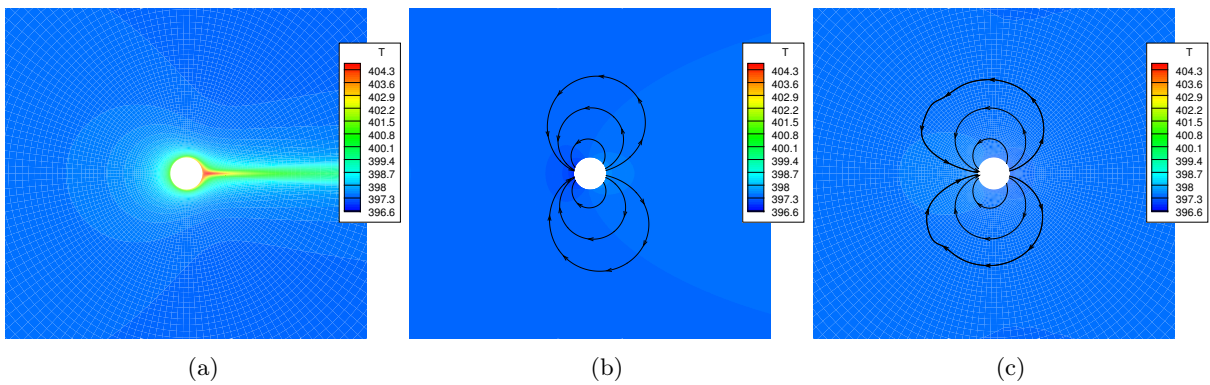


Figure 9: Temperature contours and heat-flux streamlines for subsonic flow past a circular cylinder at $Kn=0.1$ found by solving the (a) Gaussian, (b) regularized Gaussian, and (c) 14-moment closures.

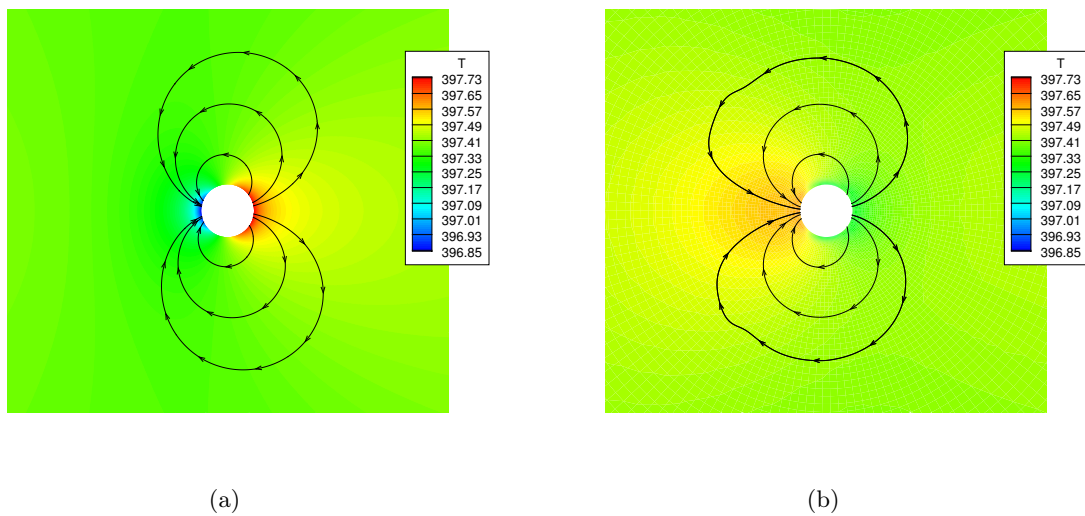


Figure 10: Temperature contours and heat-flux streamlines for subsonic flow past a circular cylinder at $Kn=0.1$ found by solving the (a) regularized Gaussian and (b) 14-moment closures. Note that the temperature contours have been rescaled to show more detail.

agreement. The temperature field for both solution methods is overall uniform, with very slight heating in front and downstream of the cylinder. The heat flux streamlines are also in good agreement, and show heat transfer from the hot to cold regions as is expected in the continuum regime. This case is a good verification of the 14-moment closure’s predictive ability for continuum regime flows in two-dimensions.

5.4.2 Results for $\text{Kn}=0.1$

Solutions found for the transition regime case, $\text{Kn}=0.1$, are presented in Figures 8, 9, and 10. For this case the Reynolds number is 0.487457. It can be seen that the Mach number contours and velocity streamlines are again very similar for each of the solution methods. The recirculation region observed in the continuum regime has disappeared, as would be anticipated for this much lower Reynolds number. The boundary layers have also become wider relative to the cylinder diameter, which is expected based on kinetic theory. A significant amount of velocity slip relative to the continuum regime solution is found above and below the cylinder. The Gaussian solution now shows very significant localized heating when compared to regularized Gaussian and 14-moment closures. This is anticipated as the Gaussian solution does not consider non-equilibrium heat transfer, which is significant in this regime. The heat flux streamlines are similar for the regularized Gaussian and 14-moment solutions, however the temperature contours differ. The regularized Gaussian shows a decrease in temperature in front of the cylinder and increased temperature behind, whereas the opposite is true for the 14-moment closure, a decrease in temperature in front of the cylinder and increase behind. Therefore, the heat flux in the 14-moment solution is oriented in the opposite direction to that expected by modelling based on the temperature gradient. This so called temperature polarization and non-gradient transport effect have been previously observed when considering flows in the transition regime, such as in analytical solutions for flow around a sphere by Torrilhon [40]. The 14-moment closure’s ability to predict this non-equilibrium phenomena is very promising, and warrants further investigation.

6 Conclusion and Future Work

A new, 14-moment, maximum-entropy-based, interpolative closure has been investigated and employed to solve a variety of canonical two-dimensional flow problems. A dispersion analysis of the 14-moment closure system has been presented which verifies the systems stability as well as demonstrating its potential to be applied to high mach number flows, through its high frozen wave speeds near the Junk subspace. The first two-dimensional solutions to this new closure have been obtained for a planar Couette flow, conduction between heated flat plates, and subsonic flow past a circular cylinder. In order to consider these cases valid boundary conditions, which accurately produce non-equilibrium phenomena, were developed based on the solid-wall half-Maxwellian boundary condition. The Couette flow results for normalized velocity and shear stress were found to be in excellent agreement with both the well established Gaussian closure and the analytical solution of Lees. The case of conduction between two heated plates resulted in a temperature jump beginning in the transition regime as expected, however there was slight discrepancy between the 14-moment solution and the Navier-Stokes solution with temperature jump boundary conditions. The results for the subsonic flow around a circular cylinder showed expected behaviours such as recirculation, velocity slip, and an increase in boundary layer thickness with increasing Knudsen number. The solutions found in the continuum regime were in good agreement with the well established regularized Gaussian closure, and the results found in the transition regime displayed temperature polarization and non-gradient transport; these interesting phenomena warrant further investigation.

Additional research into the 14-moment closure is obviously still required. Particularly, a boundary condition which is able to accurately predict phenomena associated with non-equilibrium heat transfer, such as temperature jump, is desired. Improved boundary conditions will continue to be explored by considering interior distributions which are more true to the actually 14-moment closure distribution. For instance, Grad-like perturbations of the Gaussian closure could result in more general distributions which include heat transfer considerations, while still being based upon a maximum-entropy distribution. The case of subsonic flow past a circular cylinder requires further investigation. The drag around the cylinder should be calculated and compared to experimental data in order to verify the 14-moment solution. The solutions to the 14-moment closure should also be validated by comparison with DSMC simulation results. Improved computational performance of the multidimensional solver will also be explored by replacing the semi-implicit solution method presented in Section 4.1 with an implicit Newton-Krylov-Schwarz (NKS) solver. Previous implementations of NKS with moment closures have shown savings of

a factor of 50-60 in CPU time for micro-scale flow problems [41].

Acknowledgements

Computational resources were provided by the SciNet High Performance Computing Consortium at the University of Toronto and Computer/Calcul Canada through funding from the Canada Foundation for Innovation (CFI) and the Province of Ontario, Canada. The primary author would like to thank his colleague Christopher Lam for his assistance in generating the regularized Gaussian solutions and helpful discussions.

References

- [1] C. Shen. *Rarefied Gas Dynamics: Fundamentals, Simulations and Micro Flows*. Springer, New York, 2010.
- [2] C. Ho and Y. Tai. Micro-electro-mechanical-systems (mems) and fluid flows. *Ann. Rev. Fluid Mech.*, 30:579–612, 1998.
- [3] X. Nie, G. D. Doolen, and S. Chen. Lattice-boltzmann simulations of fluid flows in mems. *J. Comput. Phys.*, 107:279–289, 2002.
- [4] F. S. Sherman and L. Talbot. Experiment versus kinetic theory for rarefied gases. In F. M. Devienne, editor, *Rarefied Gas Dynamics*, volume 3 of *International Series on Aeronautical Sciences and Space Flight*, pages 161–191, New York, 1960. Pergamon Press.
- [5] C.K. Chu. Kinetic theoretic description of the formation of a shock wave. *Phys. Fluids*, 8(1):12–22, 1965.
- [6] G. A. Bird. *Molecular Gas Dynamics and the Direct Simulation of Gas Flows*. Clarendon Press, Oxford, 1994.
- [7] L. Mieussens. Discrete velocity model and implicit scheme for the BGK equation of rarefied gas dynamics. *Mathematical Models and Methods in Applied Sciences*, 10(8):1121–1149, 2000.
- [8] C. P. T. Groth and J. G. McDonald. Towards physically-realizable and hyperbolic moment closures for kinetic theory. *Continuum Mech. Thermodyn.*, 21(6):467–493, 2009.
- [9] C. D. Levermore. Moment closure hierarchies for kinetic theories. *J. Stat. Phys.*, 83:1021–1065, 1996.
- [10] I. Müller and T. Ruggeri. *Rational Extended Thermodynamics*. Springer-Verlag, New York, 1998.
- [11] J. G. McDonald, J. S. Sachdev, and C. P. T. Groth. Application of Gaussian moment closure to micro-scale flows with moving and embedded boundaries. Accepted to the AIAA Journal, 2014.
- [12] J. G. McDonald and M. Torrilhon. Affordable robust moment closures for CFD based on the maximum-entropy hierarchy. *J. Comput. Phys.*, 251:500–523, 2013.
- [13] J. C. Maxwell. On the dynamical theory of gases. *Philosophical Transactions of the Royal Society of London*, 157:49–88, 1867.
- [14] L. Boltzmann. Weitere studien über das wärme-gleichgewicht unter gasmolekülen. *Sitz. Math.-Naturwiss. Cl. Akad. Wiss. Wien*, 66:275–370, 1872.
- [15] T. I. Gombosi. *Gaskinetic Theory*. Cambridge University Press, Cambridge, 1994.
- [16] G. N. Patterson. *Introduction to the Kinetic Theory of Gas Flows*. University of Toronto Press, Toronto, 1961.
- [17] R. D. Present. *Kinetic Theory of Gases*. McGraw-Hill, New York, 1958.
- [18] P. L. Bhatnagar, E. P. Gross, and M. Krook. A model for collision processes in gases. I. small amplitude processes in charged and neutral one-component systems. *Physical Rev.*, 94(3):511–525, 1954.
- [19] G. N. Patterson. *Molecular Nature of Aerodynamics*. University of Toronto Press, Toronto, 1981.
- [20] H. Grad. On the kinetic theory of rarefied gases. *Commun. Pure Appl. Math.*, 2:331–407, 1949.
- [21] I. Müller and T. Ruggeri. *Rational Extended Thermodynamics*. Springer-Verlag, New York, 2 edition, 1995.
- [22] S. Chapman. On the kinetic theory of a gas. part II. – a composite monoatomic gas: Diffusion, viscosity, and thermal conduction. *Phil. Trans. Royal Soc. London A*, 217:115–116, 1916.
- [23] D. Enskog. *Kinetische Theorie der Vorgänge in Massing Verdumten Gasen*. PhD thesis, University of Upsala, 1917.
- [24] J. G. McDonald and C. P. T. Groth. Towards realizable hyperbolic moment closures for viscous

- heat-conducting gas flows based on a maximum-entropy distribution. *Continuum Mech. Thermodyn.*, 25(5):573–603, 2013.
- [25] H. L. Hamburger. Hermitian transformations of deficiency-index $(1, 1)$, jacobian matrices, and undetermined moment problems. *Amer. J. Math.*, 66:489–552, 1944.
- [26] C. D. Levermore and W. J. Morokoff. The Gaussian moment closure for gas dynamics. *SIAM J. Appl. Math.*, 59(1):72–96, 1998.
- [27] S. L. Brown, P. L. Roe, and C. P. T. Groth. Numerical solution of a 10-moment model for nonequilibrium gasdynamics. Paper 95-1677, AIAA, June 1995.
- [28] J. G. McDonald and C. P. T. Groth. Numerical modeling of micron-scale flows using the Gaussian moment closure. Paper 2005-5035, AIAA, June 2005.
- [29] J. G. McDonald and C. P. T. Groth. Extended fluid-dynamic model for micron-scale flows based on Gaussian moment closure. Paper 2008-0691, AIAA, January 2008.
- [30] M. Junk. Domain of definition of Levermore’s five-moment system. *J. Stat. Phys.*, 93(5/6):1143–1167, 1998.
- [31] V. Venkatakrisnan. On the accuracy of limiters and convergence to steady state solutions. Paper 93-0880, AIAA, January 1993.
- [32] A. Harten, P. D. Lax, and B. van Leer. On upstream differencing and Godunov-type schemes for hyperbolic conservation laws. *SIAM Rev.*, 25(1):35–61, 1983.
- [33] J. A. Hittinger. *Foundations for the Generalization of the Godunov Method to Hyperbolic Systems with Stiff Relaxation Source Terms*. PhD thesis, University of Michigan, 2000.
- [34] W. G. Vincenti and C. H. Kruger. *Introduction to Physical Gas Dynamics*. R. E. Krieger Publishing, Huntington, NY, 1975.
- [35] E. H. Kennard. *Kinetic Theory of Gases*. McGraw-Hill, New York, 1938.
- [36] M. Knudsen. Die molekulare wÄdrmeleitung der gase und der akkommodationskoeffizient. *Annalen der Physik*, 339(4):593–656, 1911.
- [37] C. P. T. Groth, T. I. Gombosi, P. L. Roe, and S. L. Brown. Gaussian-based moment-method closures for the solution of the Boltzmann equation. In J. Glimm, M. J. Graham, J. W. Grove, and B. J. Plohr, editors, *Proceedings of the Fifth International Conference on Hyperbolic Problems — Theory, Numerics, Applications, University of New York at Stony Brook, Stony Brook, New York, U.S.A., June 13–17, 1994*, pages 339–346, New Jersey, 1996. World Scientific.
- [38] C. P. T. Groth, P. L. Roe, T. I. Gombosi, and S. L. Brown. On the nonstationary wave structure of a 35-moment closure for rarefied gas dynamics. Paper 95-2312, AIAA, June 1995.
- [39] J. G. McDonald. *Extended Fluid-Dynamic Modelling for Numerical Solution of Micro-Scale*. PhD thesis, University of Toronto, October 2010.
- [40] M. Torrilhon. Slow gas microflow past a sphere: Analytic solution based on moment equations. *Phys. Fluids*, 22(072001):1–16, 2010.
- [41] C. K. S. Lam and C. P. T. Groth. Numerical prediction of three-dimensional non-equilibrium gaseous flows using the Gaussian moment closure. Paper 2011-3401, AIAA, June 2011.